

Spatially-resolved nonlinearity measurements of $\text{YBa}_2\text{Cu}_3\text{O}_{7-\delta}$ bicrystal grain boundaries

Sheng-Chiang Lee and Steven M. Anlage^{a)}

Center for Superconductivity Research, and Materials Research Science and Engineering Center,
Department of Physics, University of Maryland, College Park, Maryland 20742-4111

(Received 2 October 2002; accepted 22 January 2003)

We have developed a near-field microwave microscope to locally excite a superconducting film and measure second- and third-order harmonic responses at microwave frequencies. We study the local nonlinear response of a $\text{YBa}_2\text{Cu}_3\text{O}_{7-\delta}$ thin film grown on a bicrystal SrTiO_3 substrate. The location of the bicrystal grain boundary is clearly identified by the microscope through higher harmonic response, and the spatial resolution is on the order of the magnetic loop diameter, about $500\mu\text{m}$. The harmonic power and spatial resolution are modeled with a one-dimensional extended Josephson junction simulation. From the model, the second-order harmonic response is dominated by Josephson vortex generation and flow. A geometry-free nonlinear scaling current density $J_{\text{NL}} \cong 10^4 \sim 10^5 \text{ A/cm}^2$ is also extracted from the data, indicating that the grain boundary weak link is the dominant nonlinear source in this case. © 2003 American Institute of Physics.
[DOI: 10.1063/1.1561152]

The nonlinear properties of high- T_c superconductors have been of great concern in microwave applications, although the microscopic origins of the nonlinear response still remain uncertain.¹ All superconductors have an intrinsic nonlinearity associated with the nonlinear Meissner effect (NLME). Calculations of harmonic response based on BCS theory,^{2,3} Ginzburg–Landau (GL) theory,⁴ and microwave field-induced modulation of the super/normal fluid densities near T_c ⁵ have been proposed to describe the intrinsic nonlinearities of superconductors. Extrinsic sources of nonlinearity include grain boundaries,⁶ edge effects, and weakly coupled grains.⁷ Many experiments have studied the intermodulation power,^{8,9} harmonic generation,^{10,11} or the nonlinear surface impedance of superconductors^{12,13} as a function of applied microwave power. However, most nonlinear experiments are done with resonant techniques, which by their nature study the averaged nonlinear response from the whole sample rather than locally. Such techniques usually have difficulty in either avoiding edge effects, which give undesired vortex entry, or in identifying the microscopic nonlinear sources. Therefore, a technique capable of locally measuring nonlinear properties of samples is necessary for understanding the physics of different nonlinear mechanisms. In addition, most existing experimental techniques focus on third-order nonlinearities, which can be conveniently studied by intermodulation techniques, but rarely address the second-order nonlinear response. Here, we present a technique to locally characterize second- and third-order nonlinearities through spatially localized harmonic generation.

In prior work,⁹ we studied the “local” and “global” intermodulation signal from a high- T_c superconducting microwave resonator using a scanned electric field pick-up probe. However, the local measurements were actually a superposition of nonlinear responses that were generated locally but propagated throughout the microstrip and formed a resonant

standing-wave pattern. To avoid this loss of spatial information, we have developed a nonresonant near-field microwave microscope, to nondestructively measure the local harmonic generation from unpatterned samples.

In our experiment (Fig. 1), low-pass filters are used to filter out higher harmonics generated by the microwave source, guaranteeing that only the selected fundamental frequency is sent to the sample. A loop probe, which is made of a coaxial cable with its inner conductor forming a semicircular loop shorted with the outer conductor, induces microwave frequency currents of a controlled geometry in the sample. The probe can be translated over the surface of the sample in the x – y plane. The harmonic signals generated in the sample couple back to the loop probe. An advantage of this probe is the localized and directional microwave current induced on the sample surface, which enables the study of direction-dependent nonlinearities. Reflected harmonics are selected by two high-pass filters, before being amplified by $\sim 65 \text{ dB}$, and measured by a spectrum analyzer.

The sample is a 500-\AA -thick $\text{YBa}_2\text{Cu}_3\text{O}_{7-\delta}$ (YBCO)

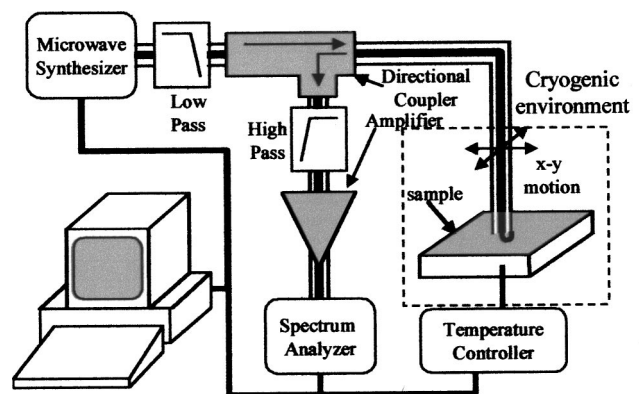


FIG. 1. Experimental schematic. The 6.5-GHz microwave signal is low-pass filtered before being sent to the sample, and high-pass filtered before being amplified and measured by the spectrum analyzer.

^{a)}Electronic mail: anlage@squid.umd.edu

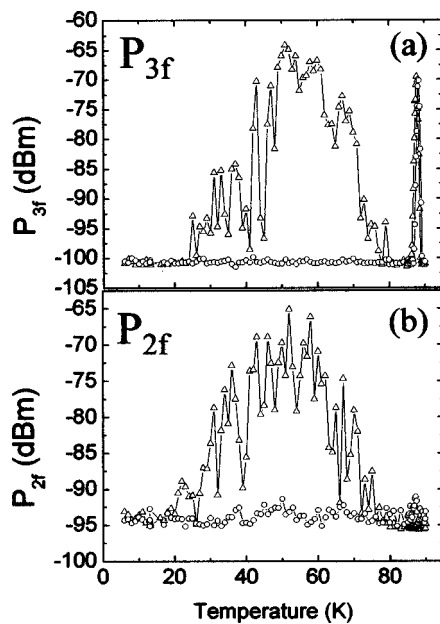


FIG. 2. Temperature dependence of (a) third-order and (b) second-order harmonic generation on non-GB YBCO surface (circles) and YBCO GB (triangles) in the temperature range 5~90 K. The fundamental frequency is 6.5 GHz and input power +8 dBm.

thin film deposited by pulsed laser deposition on a bicrystal SrTiO₃ substrate with a 30° misorientation. The distance between the probe and the sample is fixed by a 12.5- μ m-thick Teflon™ sheet. Measurements of the temperature dependent third-order harmonic power (P_{3f}) are first performed, both above the grain boundary (GB) and far from the boundary (non-GB), as shown in Fig. 2. A strong peak in $P_{3f}(T)$ is observed around $T_c \sim 88.9$ K (measured by ac susceptibility) at all locations on the sample. The $P_{3f}(T)$ peaks have similar magnitudes at both locations, although there is a slight (~ 0.5 K) shift of T_c . Note that all measurements are taken near the middle of the film, where we have verified that current-enhancement edge effects are absent.¹⁴ This peak near T_c is predicted by all models of intrinsic nonlinearities of superconductors, and the predicted power-3 dependence of the P_{3f} on the input microwave power (P_f) is observed. Note also that no feature is seen in P_{2f} near T_c , as expected for a time-reversal symmetric superconductor.

The SrTiO₃ substrate is a nonlinear dielectric at low temperatures,¹⁵ and we have measured harmonic response from bare SrTiO₃ substrates below 80 K.¹⁴ The nonlinear response is confined to narrow temperature ranges at temperatures when the substrate becomes resonant due to its temperature-dependent, high dielectric constant. At temperatures below 80 K, a strongly temperature-dependent P_{3f} is observed above the YBCO bicrystal grain boundary, while no detectable P_{3f} is seen away from the grain boundary. Additionally, temperature-dependent P_{2f} and P_{3f} at the grain boundary are measured up to 250 K, and no nonlinear response due to dielectric nonlinearity was observed. Taken together, this is evidence that the observed P_{3f} is from the grain boundary, not the nonlinearity of the SrTiO₃ substrate. Power dependencies of P_{2f} and P_{3f} were also performed at both locations at 60 K ($\ll T_c$) and 95 K ($> T_c$). As shown in Fig. 3, strongly power-dependent P_{2f} and P_{3f} are only observed above the grain boundary at 60 K, while no response

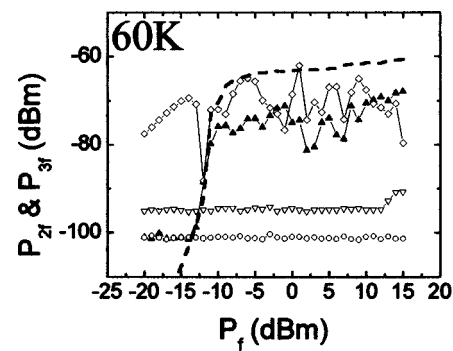


FIG. 3. Power dependence of second- and third-order harmonic generation on both non-GB YBCO surface and GB at 60 K ($\ll T_c$) (filled triangles: P_{3f} on GB; diamonds: P_{2f} on GB; circles: P_{3f} on non-GB; inverted triangles: P_{2f} on non-GB). The uncoupled ERSJ model calculation for the power dependence of the third-harmonic generation on the grain boundary at 60 K is also plotted as a dashed line for comparison.

is seen above the background noise level away from the bicrystal grain boundary.

To demonstrate that the microwave microscope is able to spatially resolve a localized source of nonlinearity, a measurement of P_{2f} and P_{3f} along a line crossing the grain boundary is performed. As shown in Fig. 4, a clear peak in both P_{2f} and P_{3f} is observed above the GB, with a width of about 500 μ m. The width of the observed P_{2f}/P_{3f} peaks are about the size of the loop probe, which determines the spatial distribution of the surface current on the sample. This interpretation is confirmed by reproducing this peak with the extended resistively shunted Josephson junction model (ERSJ) discussed later. A measurement of P_{2f} and P_{3f} along the grain boundary was also performed, and variations of both signals are observed, demonstrating our ability to resolve nonuniformity of the boundary.

It is well known that applying microwave current to a single RSJ generates harmonics at all odd integer multiples of the drive frequency.^{6,16} To obtain a more comprehensive understanding of weak-link junctions, the ERSJ model was introduced to model long Josephson junctions, such as the

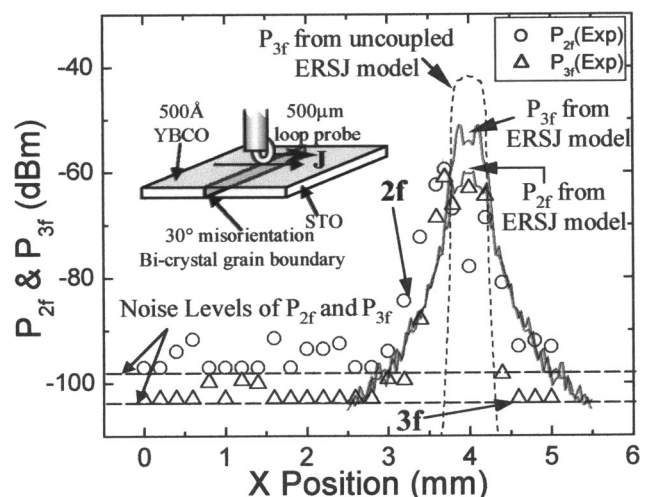


FIG. 4. Second-order (P_{2f} , circles) and third-order harmonic (P_{3f} , triangles) power along a line crossing the bicrystal grain boundary, which is located at $X=4$ mm, with input power $P_f=+8$ dBm. Calculations of P_{2f} and P_{3f} from the coupled ERSJ model are shown in solid lines, and P_{3f} from the uncoupled ERSJ in a dashed line. Inset is the schematic of the probe-sample arrangement.

YBCO bicrystal grain boundary.^{6,7,12} In this letter, we present ERSJ models to simulate a YBCO bicrystal grain boundary as either an array of identical inductively coupled, or independent (uncoupled), Josephson junctions acting in parallel. From prior work with these junctions, we expect each junction¹⁷ in the ERSJ model to have a Josephson penetration depth $\lambda_J \sim 3 \mu\text{m}$, a critical current of $8 \mu\text{A}$, and a shunt resistance of 20Ω . The currents applied to each junction vary according to the surface current distribution on the film induced by the loop probe. We sum up the nonlinear potential differences across all junctions, and extract the higher harmonics from this collective nonlinear potential difference via Fourier expansion.⁶ The spatial distribution of the surface current density is calculated from a simplified analytical model of an ideal circular loop in a vertical plane, with radius $270 \mu\text{m}$, coupling to a perfectly conducting horizontal plane $382.5 \mu\text{m}$ away from the center of the loop. The magnitude of the current density is determined by a much more sophisticated microwave simulation, which also produces a similar surface current distribution.

The calculation of P_{3f} in the uncoupled ERSJ model is shown as the dashed line centered on 4 mm in Fig. 4. This model predicts a narrow distribution of P_{3f} of greater magnitude (almost 20 dB) than is observed experimentally. It also predicts no P_{2f} , due to the absence of Josephson vortices in this model. A power dependence calculation from this uncoupled ERSJ model is also performed and compared with experimental results (dashed line in Fig. 3). The comparison shows qualitative agreement with the $P_{3f}(P_f)$ data. On the other hand, numerical calculations with the inductively coupled ERSJ model, which includes Josephson vortices, give a very good description in both magnitude and spatial resolution of the experimental results for both P_{2f} and P_{3f} (solid lines in Fig. 4).

To further evaluate the capability of our microscope to detect intrinsic superconducting nonlinearities due to different mechanisms, we extract a geometry-free scaling current density J_{NL} ,⁸ from our data. We assume that the quadratic nonlinearity in the kinetic inductance of our sample dominates the nonlinear response through $L_{\text{KI}} \equiv (\mu_0/I^2) \int_{\text{volume}} \lambda_L(T, J)^2 J^2 dV \equiv L_0 + \Delta L I^2$, and $P_{3f} = (\omega \Delta L I^3/4)^2/2Z_0$, where P_{3f} is the third-harmonic power in the sample, ω and I are the microwave frequency and current, respectively Z_0 is the characteristic impedance of the transmission line, L_{KI} is the kinetic inductance of the sample, L_0 and ΔL are the linear and second-order nonlinear terms in L_{KI} , respectively, $\lambda_L(T, J) = \lambda_L(T, 0) \{1 + [J/J_{\text{NL}}(T)]^2\}^{1/2}$ is the temperature- and current-dependent London penetration depth, and J_{NL} is the nonlinearity scaling current density. Different microscopic models of nonlinearity predict different values and temperature dependences of $J_{\text{NL}}(T)$. For example, in the NLME and GL theory, $J_{\text{NL}} \sim 10^8 \text{ A/cm}^2$ or higher,^{4,8} except for temperatures close to T_c , while the J_{NL} of a long, one-dimensional Josephson junction array is expected to be about 10^6 A/cm^2 or less.⁸ We follow Booth's algorithm¹⁸ to calculate the nonlinear term in the inductance, and the expected third-order harmonic response, all as a function of J_{NL} , using the current distribution calculated from the model of the loop probe.

Assuming $\lambda_L(T=0, J=0) = 1500 \text{ \AA}$, we obtain the J_{NL} calculated near the grain boundary at 60 K to be $J_{\text{NL}}^{\text{GB}} \sim 1.5 \times 10^5 \text{ A/cm}^2$, while the sensitivity of our setup is currently limited to $J_{\text{NL}} \leq 1.3 \times 10^6 \text{ A/cm}^2$.¹⁴ However, the model calculation suggests that thinner films and stronger coupling between the film and probe will give stronger nonlinear response from a given mechanism, and improve the sensitivity to nonlinearities associated with larger values of J_{NL} .

We have created a near-field microwave microscope that is capable of locally measuring nonlinear microwave behavior, thus providing an important alternative tool to study nonlinearities of superconductors. The spatial resolution is determined by the size of the loop probe, which is about $500 \mu\text{m}$ in the current setup, and can be improved by reducing the size of the loop and decreasing the loop/sample separation. A quantitative understanding of the magnitude and spatial resolution of the second- and third-order harmonic response is well achieved by the coupled ERSJ model. A geometry-free scaling current density J_{NL} is extracted from our measurement, and can be used to further study the physics of different nonlinearities of superconductors.

We thank S.-Y. Lee for making the YBCO thin films, and G. Ruchti for the current calculation. This work is supported by DARPA DSO contract No. MDA972-00-C-0010 through a subcontract by STI, the Maryland/Rutgers NSF MRSEC under grant DMR-00-80008 NSF IMR under grant DMR-98-02756, and NSF-GOALI DMR-0201261.

¹M. Hein, *High-Temperature-Superconductor Thin Films at Microwave Frequencies* (Springer, New York, 1999), pp. 103–238.

²S. K. Yip and J. A. Sauls, Phys. Rev. Lett. **69**, 2264 (1992).

³T. Dahm and D. J. Scalapino, J. Appl. Phys. **81**, 2002 (1997).

⁴J. Gittleman, B. Rosenblum, T. E. Seidel, and A. W. Wicklund, Phys. Rev. A **137**, A527 (1965).

⁵I. Ciccarello, C. Fazio, M. Guccione, and M. Li Vigni, Phys. Rev. B **49**, 6280 (1994).

⁶J. McDonald and J. R. Clem, Phys. Rev. B **56**, 14723 (1997).

⁷D. E. Oates, Y. M. Habib, C. J. Lehner, L. R. Vale, R. H. Ono, G. Dresselhaus, and M. S. Dresselhaus, IEEE Trans. Appl. Supercond. **9**, 2446 (1999).

⁸B. A. Willemsen, K. E. Kihlstrom, T. Dahm, D. J. Scalapino, B. Gowe, D. A. Bonn, and W. N. Hardy, Phys. Rev. B **58**, 6650 (1998).

⁹W. Hu, A. S. Thanawalla, B. J. Feenstra, F. C. Wellstood, and S. M. Anlage, Appl. Phys. Lett. **75**, 2824 (1999).

¹⁰C. Wilker, Z.-Y. Shen, P. Pang, W. L. Holstein, and D. W. Face, IEEE Trans. Appl. Supercond. **5**, 1665 (1995).

¹¹E. E. Pestov, Y. N. Nozdrin, and V. V. Kurin, IEEE Trans. Appl. Supercond. **11**, 131 (2001).

¹²P. P. Nguyen, D. E. Oates, G. Dresselhaus, and M. S. Dresselhaus, Phys. Rev. B **48**, 6400 (1993).

¹³I. Ciccarello, C. Fazio, M. Guccione, and M. Li Vigni, Ann. Phys. (Leipzig) **3**, 13 (1994).

¹⁴S.-C. Lee and S. M. Anlage, IEEE Trans. Appl. Supercond. (in press); cond-mat/0210102, (2003).

¹⁵E. I. Golovenchits, V. A. Sanina, and A. V. Babinskii, JETP Lett. **63**, 674 (1996).

¹⁶T. Van Duzer and C. W. Turner, *Principles of Superconductive Devices and Circuits* (Prentice Hall, Upper Saddle River, NJ, 1999), pp. 206–212.

¹⁷In the ERSJ model, each junction has a width λ_J , coupled by a lateral inductance of 10^{-10} H . The circuit is identical to that in Ref. 7.

¹⁸J. C. Booth, J. A. Beall, D. A. Rudman, L. R. Vale, and R. H. Ono, J. Appl. Phys. **86**, 1020 (1999).